Open Ceramics 15 (2023) 100427



Contents lists available at ScienceDirect

Open Ceramics

journal homepage: www.sciencedirect.com/journal/open-ceramics





Mineralogical and microstructural characterization of ceramics from the fifth and fourth millennium BC in the central plateau of Iran

Maria Daghmehchi [a,*], Chiara Coletti [b], Dong Hyeok Moon [c], Mohammad Esmaeil Esmaeili Jelodar [d], Hadi Omrani [e], Arianit A. Reka [f], Ali Nematollahzadeh [g], Mohammadamin Emami [h]

[a] Department of Archaeology and History of Art, Koç University, 34450, Istanbul, Turkey
[b] Department of Geosciences, University of Padova, Via G. Gradenigo 6, 35131, Padova, Italy
[c] Conservation Science Division, National Research Institute of Cultural Heritage, Daejeon, 34122, South Korea
[d] Department of Archaeology, Faculty of Literature and Humanities, University of Tehran, 1417614418 Tehran, Iran
[e] Department of Geology, Faculty of Sciences, Golestan University, Gorgan, Iran
[f] Faculty of Natural Sciences and Mathematics, University of Tetovo, Ilinden N.n., 1200, Tetovo, Macedonia
[g] Department of Chemical Engineering, University of Mohaghegh Ardabili, Ardabil, Iran
[h] Art University of Isfahan, Department of Conservation, Isfahan, 1744, Iran

ARTICLE INFO

Handling Editor: Dr P Colombo

Keywords:
Ceramic
Pore size distribution
Crushing strength
Sintering process

ABSTRACT

This research presents the effects of sintering process and clay composition on the physico-mechanical properties of ceramics from the fifth and fourth millennium BC (6950 ± 280 to 5040 ± 220 TL dating). The combined multiscale mercury intrusion porosimetry (MIP) revealed the increase of round cryptopores and ultramicropores in a range of 0.01–0.1 μm and 0.1–5 μm respectively, closely linked to vitrified glassy connections and bonding between particles and the partial melting of phyllosilicates with different sizes of bubbles at 950 °C. Cold crushing strength (CCS) of the ceramics, containing high calcite and phyllosilicate mineral exhibited a lower strength value from 6.24 to 6.31 MPa at ~750–800 °C due to the increase in crack porosity area with high interconnectivity and internal stresses. However, the ceramics with a well glassy network show a higher strength value of 16.5Mpa, contributing to sustainable ceramic materials with a uniform cross-section >900 °C and minimal shrinkage for conservation treatment.

1. Introduction

Testing the mechanical resistance, mineralogy and porosity of the wares can provide significant evidence of technological changes. The study of fracture strength clearly reveals the effect of technological choices on the long-term stability of vessels [1,2]. Mechanical behavior depends on the total porosity as well as pore structures which is deeply affecting the strength, bulk density, surface area, and thermophysical behavior of building materials and ceramics [3–6]. The porosity of ceramics is greatly influenced by the firing conditions, the presence of distinct minerals, the grain size distribution, temper shape, chemical compositions, the microstructural characteristics, and forming process [3,6–10]. Mercury intrusion porosimetry)MIP(is a well-established method for porosity measurement in a very large range of pore sizes, nominally between 6 and 10,000 nm [11,12]. Furthermore, a low-pressure porosimeter also enables us to measure the entire pore sizes which are outside of the range of this porosimeter. A combined multiscale MIP is a major parameter for evaluating the porous structure of ceramics and significantly estimates the distribution of micropores >5 nm. Conversely, the backscattered electron (BSE) image of Field Emission-Scanning Electron Microscope (FESEM) analysis was used to estimate the macropore content. FE-SEM is a very convenient tool for porosity measurements of ceramic material and reveals the shape, distribution, and connectivity of macropores (pore radius >1 μm) [13–15].

This research investigates the influence of the pore size distribution and the microstructure on the cold crushing strength of ceramics at different sintering processes. For this purpose, a combination of two porosimeter systems was used to evaluate the entire pore radius range from 3.7 to 7500 nm and 2.8–140 μm. The ceramics from the fifth to fourth millennium BC, fired at different firing conditions, behave very

* Corresponding author.
E-mail address: mdaghmeh22@ku.edu.tr (M. Daghmehchi).

https://doi.org/10.1016/j.oceram.2023.100427
Received 25 March 2023; Received in revised form 2 July 2023; Accepted 1 August 2023
Available online 2 August 2023
2666-5395/© 2023 The Authors. Published by Elsevier Ltd on behalf of European Ceramic Society. This is an open access article under the CC BY license (http://creativecommons.org/licenses/by/4.0/).

differently in pore structures. Thus, the ceramics were initially subjected to X-ray diffraction (XRD), Fourier transform infrared (FT-IR), and thermogravimetry and differential thermal analysis (TGA-DTA) to determine the phase transitions and firing temperature effect on the porous ceramics. Then, the microstructural characterization of the ceramics was carried out in order to investigate the different sintering temperatures. Finally, cold crushing strength was performed on the same samples to investigate the influence of porosity on the mechanical strength of the ceramic wares.

2. Materials and methods

2.1. Materials

Small fragments of four characteristic ceramic wares with different compositions and firing conditions were selected. These prehistoric ceramics are characterized by painted black-on-red jars and bowls and cream painted bowl and described as Mulavi Site (MS) and their context numbers (Fig. 1). The ceramic wares were taken from the archaeological site of Mulavi Street in Tehran and dated to the fifth millennium BC (Thermoluminescence (TL) dating: 6950 ± 280 and 6870 ± 300) and fourth millennium BC wares (TL dating: 5040 ± 220 and 4970 ± 420) (Iranian conservation research center, 2016). The archaeological excavation from the burial context provided the first possible evidence of the Pottery Neolithic Period in the Iranian Central Plateau. The characteristic black-on-red ware of the Cheshmeh Ali type, dating to the late sixth to mid-fifth millennia BC indicates Neolithisation from the Zagros eastward [16]. The coarse fabric cream wares were found from the lower stratigraphic sequence in Trench. VI also represents the ceramic production in the late fourth millennium of the site.

2.2. Methods

2.2.1. Mineralogical and chemical analyses

XRD analyses were performed to characterize mineralogy in the studied samples using a Philips W1800 instrument (Cu-Kα radiation, operating at 40 kV, 30 mA).

To access the structural and chemical transition of mineral phases, the FTIR spectrum was performed with a PerkinElmer Spectrum™ 100 FT-IR, with a spectral range of 4000 to 500 cm^{-1} at a resolution of 4 cm^{-1} (Iran Mineral Processing Research Center).

The mineral thermal transformation was investigated by DTA-TGA in the 30–1000 °C temperature range, using an air atmosphere with a heating rate of 10 °C min^{-1}, using NETZSCH STA 409 PC Lux model (IMPRC Laboratory).

2.2.2. Microstructure and porosity

The microstructural characterization of large through pores (in the range of >50 μm) was measured by scanning electron microscope (VEGA/TESCAN-XMU with BSE Detector and In-Beam BSE Detector), with operating conditions at an accelerating voltage of 15 kV to provide more resolution. However, the cryptopores and ultramicropore structures were also qualitatively analyzed by FE-SEM with spatial resolution below 1.00–0.50 nm (Razi Applied Science Foundation, Tehran, Iran). FESEM observations of all specimens were performed on the surface part in order to observe a clear reaction intensity of the fired earthenware bodies.

The pore size distribution of the ceramics was analyzed by applying a combined porosimetry measurement in a range from nanometer to micrometer scale in order to access a wider range of pore size: Carlo Erba Porosimeter 2000 equipment was employed to evaluate pore radius in the range from 3.7 to 7500 nm (0.003–7.5 μm) and pore volume in the range from 0.1 to 500 mm^3/g. Therefore, greater pressure will be required to intrude mercury into the smaller pore throat [12]. This porosimeter generates a contact angle of 141.3° and a surface tension of 480 dyne cm^{-1} determining the cryptopores (0.01–0.1 μm) and ultramicropores (0.1–5 μm) [17]. However, larger through pores in low-fired ceramics are not within the detection range of this porosimeter measurement. To access the distribution of larger pores, low pressure porosimetry measurement (Pascal 140) was used. This technique evaluates pore-size distribution in the range from 2.8 to 140 μm, thus including micropores (5–30 μm), mesopores (30–75 μm), and macropores (80–100 μm) [17]. The degassing process of the samples was performed at temperatures ranging from 25 to 300 °C to reveal more microporous nature [18]. This porosimeter system measures the total porosity, total cumulative volume, average pore diameter, throat size, specific surface area, and bulk and an apparent density (δg). The total volume of pores (porosity) refers to all closed, open, and interconnected pores, while total porosity is the volume portion of voids with respect to the total volume of the ceramic sherd [7,14]. The equivalent pore throat diameter, determined by intruded mercury is followed by Ref. [19] equation:

$$D = -4\gamma \cos\theta / P$$

where γ is the mercury surface tension (480 Nm), θ is the mercury contact angle (141.3°) and P is the pressure exerted [20]. The [19] equation determines pore diameter from 0.0037 to 7.5 μm.

2.2.3. Cold crushing strength (CCS)

The mechanical behavior of the ceramics was evaluated by the crushing test. Crushing strength was determined by crushing regular

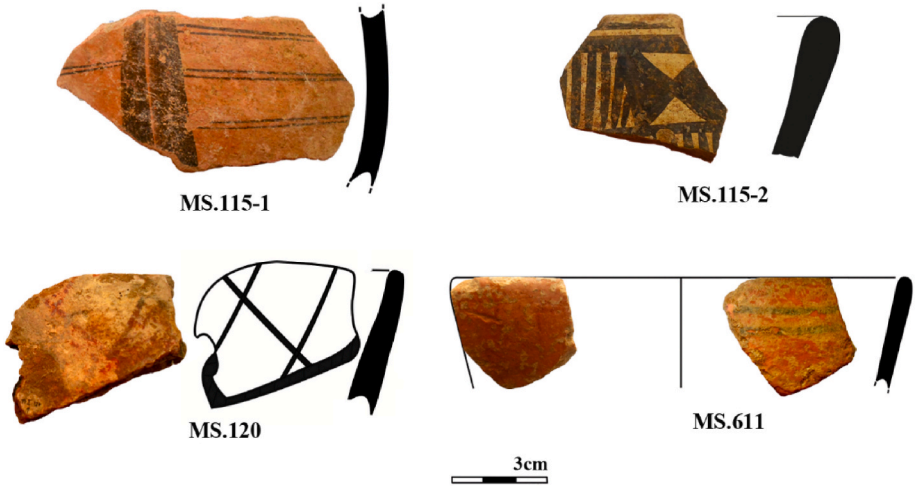


Fig. 1. Images of the ceramic samples from the fifth and fourth millennium BC in the archaeological site of Mulavi Street, Tehran.

specimens of the ceramic body sherds in dimensions 24 × 30 mm using a computer-controlled universal testing machine (Instron 8874, UK) with a ramp rate of 0.5 mm min^{-1} (Gheisari et al., 2015). The CCS of the ceramic sherds was applied according to the ASTM C 133 standards. This technique enables us to investigate the influence of the pore size distribution on the strength of the ceramics.

3. Results

3.1. Mineralogy and mineral phase transition analysis

3.1.1. XRD analysis

The studied ceramic wares mainly consist of quartz, albite, calcite, illite, calcium oxide, anorthite, and gehlenite mineral assemblage (Fig. 2). The XRD analysis indicates the moderate intensity of calcite reflection at 3.03 Å in the low-fired ceramic (sample MS.120), the formation of amorphous constituent mineral in moderate-fired ceramic (sample MS120) and the initial crystalization of new silicate phases in the high-fired ceramics such as anorthite (sample MS.115–1) as well as diopside and gehlenite (sample MS.115–2), formed by the reaction between CaO and silica and alumina during the firing process in which the transition between the complete dissolution of the $CaCO_3$ and the formation of new calcium silicate takes place (Rathossi and Pontikes, 2010; [21]. Calcite was the main constituent mineral with a thin platy structure in sample MS.120 confirmed by the sharp high-intensity reflection at 3.03 Å. It undergoes extensive structural degradation during the heating process at 750 °C, contributing to the development of secondary porosity. A small amount of illite within sample MS.120 leads to the development of more heat cracks during the lower firing process. It indicates that the mesoporosity of the samples was greatly influenced by the mineral phase transitions. The predominant reflection of calcite at 3.03 Å became less intense in sample MS.611 which is also demonstrated by FT-IR and TGA-DTA (see sections 3.1.2 and 3.1.3). The reflection of calcite in this sample is entirely disappeared, indicating a complete breakdown of calcite and the increase of CaO concentration at 800 °C. In sample MS.611, the crystal structures within the vitrified matrices generate a large pore mouth (e.g. Ref. [18]. Gehlenite was the poorly-crystalized phase in the sample MS.611, vitrified at ~800 °C. A more intense reflection of gehlenite appeared at 2 θ:31.39 ° in the sample MS.115–2 and was produced by the reaction of CaO from decomposed calcite and Al and Si from the decomposition of the clay mineral at around 850–900 °C [14]; Majerova' et al., 2018). Low-temperature gehlenite as a metastable mineral contributed to the creation of new phases such as diopside with increasing firing temperature at ~900 °C. The predominance of diopside instead of gehlenite in this sample can be related to the presence of clay minerals, fine-grained calcite, and/or the initial magnesite or dolomite content within the raw material mixture (Rathossi and Pontikes, 2010; and references therein).

The low intensity of anorthite in the sample MS.115–2 indicates its initial formation at 950 °C due to the reaction of CaO with gehlenite. Anorthite and very weak reflection of hematite were also attested in sample MS.115–1, suggesting a higher firing temperature around 900–950 °C. Fe^{3+} is incorporated in the structure of ferrian aluminian diopside and gehlenite and prevents the crystallization of hematite within the ceramic matrices [23]. It indicates an oxidation environment due to the conversion of Fe^{3+} into hematite [24]. Hematite is able to nucleate as nano-sized particles when decomposed carbonate reacts with the amorphous phase to produce diopside and gehlenite [25]. Weak reflection of hematite has been observed in MS.115–1 and MS.115–2 which was clearly distinguishable from sharp and narrow bands of primary hematite [26]. It indicates that the crystallization of hematite was limited and started above 800 °C [23].

3.1.2. Fourier-transform infrared spectroscopy (FTIR)

FTIR analysis serves as a powerful analytical tool for understanding the material composition and firing temperature ranges. In low-fired ceramics, FTIR analysis helps in detecting organic residues such as binders or additives used in the production of potteries. The weak bands of organic content only appeared in the low-fired sample MS.120 at around 2427 cm^{-1}, due to CH and C–NH^{3+} Cl− stretching mode [27]. The broad band around 3500 cm^{-1} and ~1600 cm^{-1} in this sample are assigned to the *O*–H stretching and HOH deformation domain of water molecules [28]. In this sample, the sharp absorption bands appeared around 1424 cm^{-1} due to CO_3^{-2} stretching and 871 cm^{-1} due to CO_3^{-2} bending, indicating the dissolution of primary calcite from 600 to 650 °C [29]. While initial unreacted calcite mainly appears in a lower wavenumber at ~1408 cm^{-1}. The continuous reduction of the carbonate band starts from 650 °C and completely disappears above 800 °C. In sample MS.120, slightly narrow Si–O stretching bands at ~1034 cm^{-1} and 1028 cm^{-1}, are attributed to dioctahedral mica (illite) which is also demonstrated by the high reflection of illite at ~10 Å [23]. It indicates that the firing temperature did not certainly exceed the complete destruction of the clay minerals at around 750 °C.

In moderate-fired ceramic (sample MS.611) the progressive

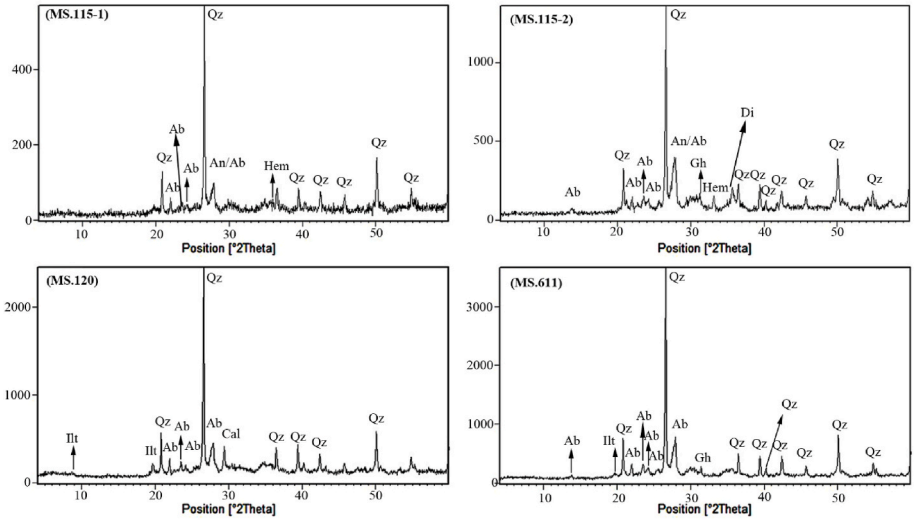


Fig. 2. XRD patterns of the ceramics, showing a progressive deterioration and conversion of calcite into calcium Oxide in samples MS.120 and MS.611 and the weak crystallization process of amorphous phases of gehlenite and anorthite in samples MS.115–1 and MS.115–2. Abbreviations: Qz: quartz, Ab: albite, An: Anorthite, Di: diopside, Gh: gehlenite, Hem: Hematite, Ilt:illite, Ca1 calcite [22].

weakening of CO_3^{-2} stretching band, shifting to a higher wavenumber indicates a higher extent of carbonate dissolution with increasing temperature at around 800 °C. In the sample MS.611 the low intense deformation bands at 875 cm^{-1} and 2512 cm^{-1} indicate a firing temperature lower than the decarbonation range at 750 °C (Fig. 3). The intensity of the asymmetric deformation band at 875 cm^{-1} and the C–O stretching vibration (V_{C-O}) of calcium carbonate at ~2516 completely disappeared above 800 °C [23]. While, the incomplete decarbonation reaction in sample MS.611 indicates that the fired ware did not completely reach the highest range of decarbonation temperature. Additionally, a very weak *Si*–O asymmetric stretching vibration of ~1086 cm^{-1} in this sample shows the appearance of amorphous calcium carbonate (ACC) due to the diffusion of CO_2 [30].

In high-fired ceramics (samples MS.115–1 and MS.115–2), the narrow *Si*–*O*–Si stretching band centered ~1038 cm^{-1} can be assigned to silicate phases [31]. A slight broadening of the *Si*–O bands in samples MS.115–1 and MS.115–2 indicates the initial sintering process at ≤ 850 °C. The Si–O stretching band shifted to a higher wavenumber of around 1067 cm^{-1} at 800 °C, and 1086 cm^{-1} at 850/900 °C in the high-fired samples MS.115–1 and MS.115–2, respectively [32,33]. The asymmetric *Si*–O band centered at ~1060 cm^{-1}, indicates a firing temperature at > 800 °C, favoring the sintering process, and the crystallization of Ca–Al-silicate minerals such as diopside, gehlenite and anorthite [21,23]. A weak crystallization of new silicates is also attested through XRD analysis. Gehlenite was observed in asymmetrical stretching of (Si, Al)O3 at ~925 cm^{-1} and diopside at ~970 cm^{-1} [25, 31].

3.1.3. -DTA analysis

At the temperature range from ~110 to 200 °C, the porosity characteristics of ceramics increased during the removal of 5% of the adsorbed water within the clay matrices and hygroscopic water from illite and organic matter [34]. The slight slope between 400 and 550 °C is consistent with similar dehydration and dehydroxylation rate of amorphous minerals in all samples (Fig. 4). However, the mass loss was more intense in sample MS.120 with porous microstructure which indicates the combustion of organic materials and decomposition of primary calcite found in the sample [35]. The TG curves indicate a continuous weight loss up to 750 °C at a heating rate of 10 °C/min. The total weight loss of around 45% contributed to the higher extent of porosity within the ceramic samples. The mass loss became less noticeable above 750 °C which indicates a complete breakdown of the crystalline phase of calcite content. A very slight exothermic event occurred around 850 and 950 °C which implies a weak crystallization process. It indicates that the amorphous remains of new silicates such as gehlenite ($Ca_2Al_2SiO_7$) and diopside ($Ca(Mg,Fe)Si_2O_6$) were formed due to the reaction of CaO with silicates from 800 to 950 C (Bayazit et al., 2016; [29]. CaO reacts with gehlenite and forms anorthite at around 950 C during the production process [23].

3.2. Microstructure and porosity

3.2.1. Field emission scanning electron microscopy (FE-SEM)

Backscattered electron (BSE) images of Field Emission-Scanning Electron Microscope (FE-SEM) allowed determining the connectivity and morphology of the pores and their response to the firing temperature in high magnification images of a certain area of the sample (Santos et al., 2012; [7].

Microstructures of samples confirmed XRD results. Samples 1 and 2 (MS.115–1 and MS.115–2, respectively), indeed, are characterized by more advanced sintered systems, than those analyzed in samples 3 and 4 (MS.120 and MS.611, respectively). It is due to the different firing temperatures reached, higher in the production of samples MS.115–1 and MS.115–2 as attested by the initial crystalization of a new phase. Sample MS.120 shows low compactness without the presence of interconnection bridges between mineral grains. Illite grains are still present showing exfoliation along basal plane sheets due to dihydroxylation and loss of OH^- (see Fig. 5 a-e) [3]. All these features and a pore system characterized by jagged pores confirmed a low degree of mineralogical and microstructural evolution and thus firing temperatures comprised between ~700 °C and 750 °C. In this sample, the highest porosity is caused by a large number of fibrous pores during the firing process (Fig. 5b). The sixth-millennium ceramics were tempered by rice straws as a chief through a pore-forming agent to improve thermal performance (Aouba et al., 2016). The addition of different organic materials leads to the generation of crack and fibrous porosity in the form of irregular channels around 400–500 °C, interconnecting with increasing firing temperature.

Additionally, the occurrence of coarse compounds within sample MS.611 contributed to the higher crack porosity as both interconnected and corona-shaped pores due to thermal expansion [36]; Hein et al., 2018). Plagioclase feldspar transformation is incipient along

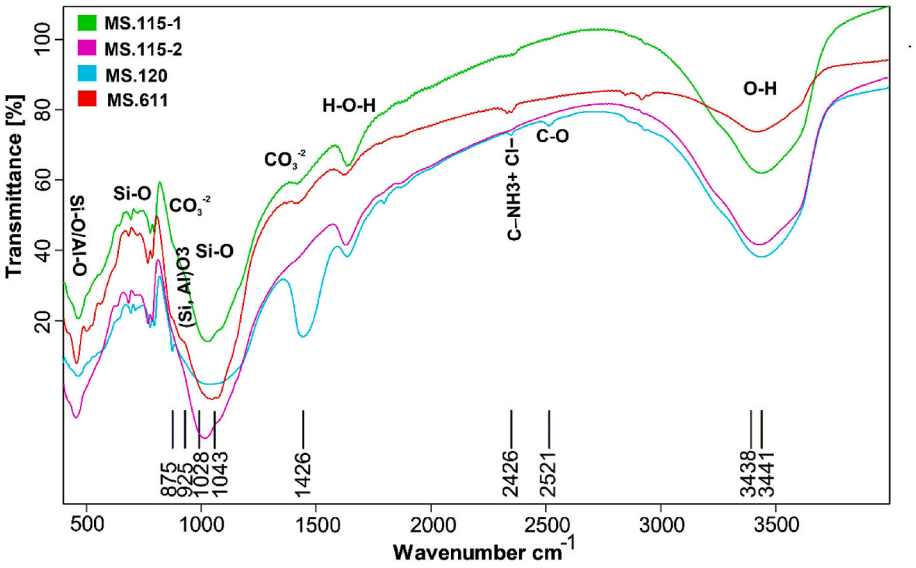


Fig. 3. FTIR spectra of the ceramic samples, showing the vibrational transition of the C–O and CO_3^{-2} carbonate bands and the *Si*–O vibrations of silicate phases at different types of ceramic samples for defining the firing temperature and composition of ceramics.

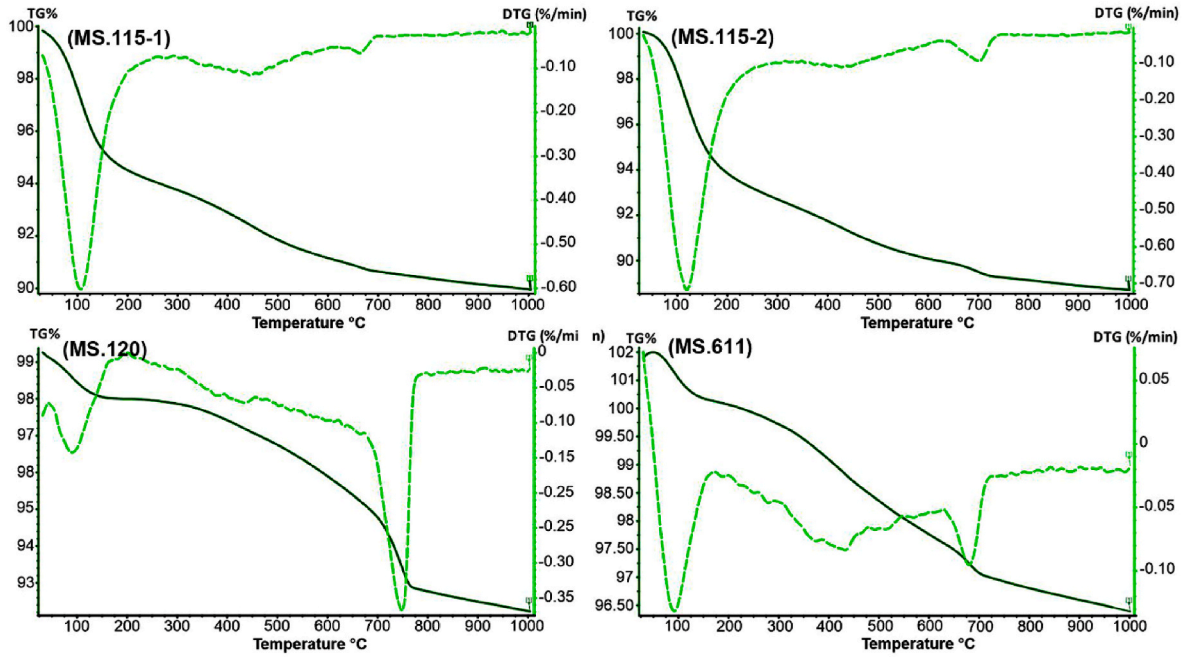


Fig. 4. TGA and DTG thermograms showing the maximum limit of firing temperature of the ceramics (T > 850 °C for the samples MS.115–1 and MS.115–2 and T < 750 °C for the sample MS.120 and ~750–800 °C for the sample MS.611). The sharp endothermic peak in the sample MS.120 indicates the high dissolution stage of coarsely crystalline calcite at 750 °C and very weak exothermic peaks >850 °C attributed to the initial crystallization of new Ca–Al-silicate phases.

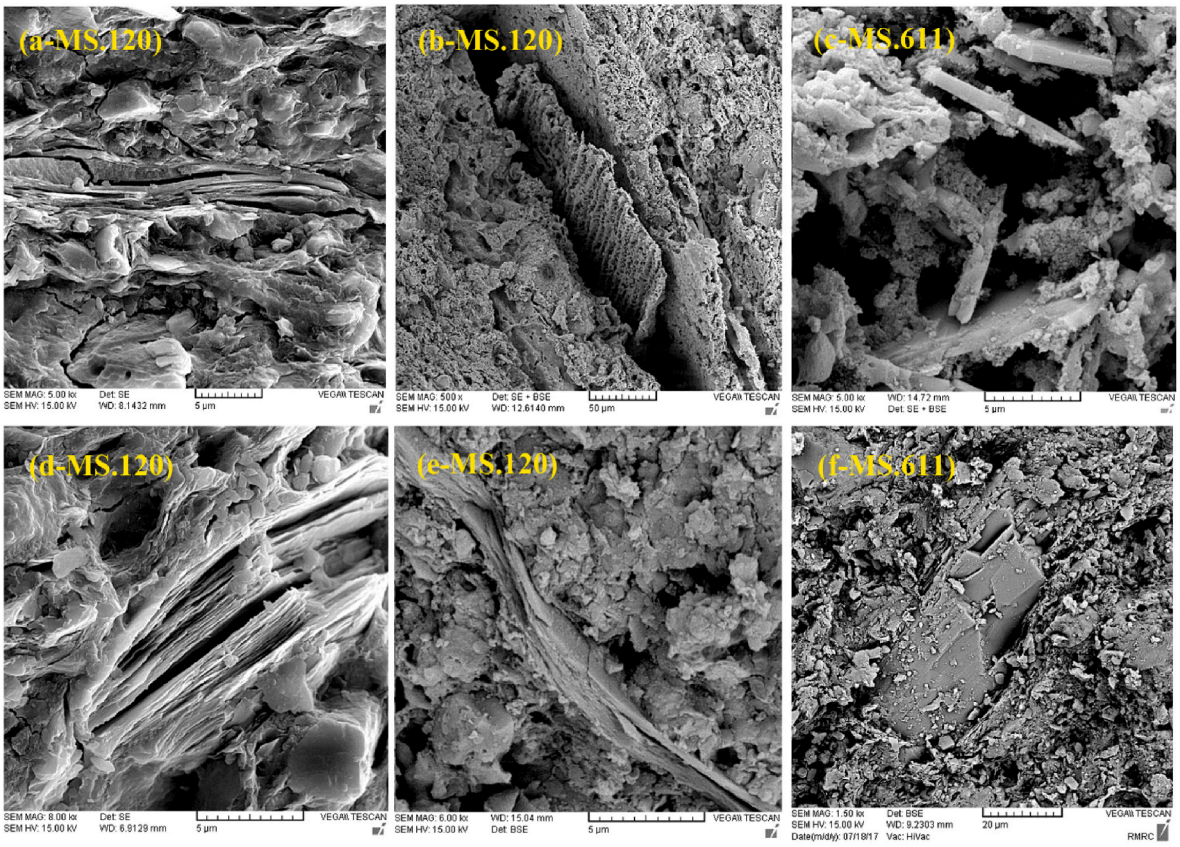


Fig. 5. SEM photomicrographs of jagged pores within and around the phyllosilicate grains in the coarse wares of MS.120 and MS.611 showing a low degree of evolution and dihydroxylation of mineral phases around 750 °C.

preferential surfaces (Fig. 5f) but without reaction rims. The circular crack porosity around the phyllosilicate grains (Fig. 5f) and within the matrix was generated at 750 °C due to the high internal stresses. The crack porosity and inter-particle voids within the clayey matrices also extended during the cooling process due to the varying thermal expansion coefficients and/or derived from decay during post-depositional effects [7,37]. The large crack and space between the mineral particles exhibited a wide variation in pore sizes, and leads to a high degree of biological and chemical alteration within the materials (Santos et al., 2012). Nonetheless, sample MS.611 has more developed microstructures and contains less total cumulative volume (57 mm^3/g) mainly derived from bubbles porosity, and cleavages and grain have evidence of reaction (Fig. 6b).

Samples MS.115–1 and MS.115-2 show a developed microstructure, with the presence of reaction grain rims and interconnection bridges between crystals. The ground matrix shows cellular-type and isolated pores, generally rounded, suggesting at initial vitrification of the clay body and, therefore, a firing temperature above 850 °C [8,38]. The round pore structure, smaller than 0.005 μm, increases greatly due to the partial melting of phyllosilicates from 950 °C with different sizes of bubbles. The formation of a glassy phase increases ultramicropores (0.1–5 μm), leads to a less porous structure [39] (Fig. 6c and f), and decreases the interconnectivity of the pores [40,41]. Samples MS.115–1 and MS.115-2 showed a large number of ultramicropores and a high extent of vitrification [9] (Fig. 6a).

3.2.2. *Mercury intrusion porosimetry*

Porosity measured in samples MS.115–1 and MS.115–2 (by means Carlo o Erba Porosimeter 2000 equipment) displays a nanopore abundance of 8.00 and 5.00%, respectively (Table 1) and indicates an abundance of cryptopores in the structure. Pore diameters below 0.05 μm suggested partial sintering of clay minerals and a firing temperature >950 °C. Pore coarsening also occurred at high sinter processing due to interconnection bridges formed between the crystal grains structures [42]. In both samples, pores are distributed in a narrow range (between 0.008 and 0.025 μm) 8–50 nm (Fig. 7). The intrusion curve shows a greater share of the cryptopores in the fine fabric ceramic, sintered at 950 °C. The cryptopores and ultramicropores increased at 950 °C due to the formation of glassy phases with bubbles, determined by FE-SEM analysis. The high-sintered ceramics show a very low porosity of <10% with a great decrease in cumulative pore volume (PCV = ~0.20 mL/g) depending on their glassy microstructure [36] (Fig. 7).

Table 1
Porosity, the pore volume, measuring different pore ranges and crushing strength of the studied ceramics (No.: 1 to 4).

Sample	MS.115-1	MS.115-2	MS.120	MS.611
Total porosity (%)	8.00	5.00	19.96	5.67
Total PCV (mL/g)	0.16	0.11	68.26	57.62
CCS (MPa)	9.41	16.5	6.24	6.31
Fracture Energy (N/m)	6926	10,424	2635	4413
Firing Temperature	850 °C	≥850/~900 °C	<700 °C	~750 °C

PCV: cumulative pore volume; CCS: Cold Crushing Strength.

The sample MS.120 from the fifth millennium BC (measured by means Pascal 140 equipment) was dominated by large through pores due to the burning of organic materials [15] and the decarbonation process which calcite generates a more porous matrix [10]. The pores resulting from organic matter may exhibit distinct organic shapes such as the remnants of plant fibers or cellular structures, whereas pores from mineral dissolution may show irregular shapes (Fig. 5b). This is particularly evident in the sample MS.120 through FE-SEM and TGA-DTA analyses in which the decomposition of carbonate is still occurring

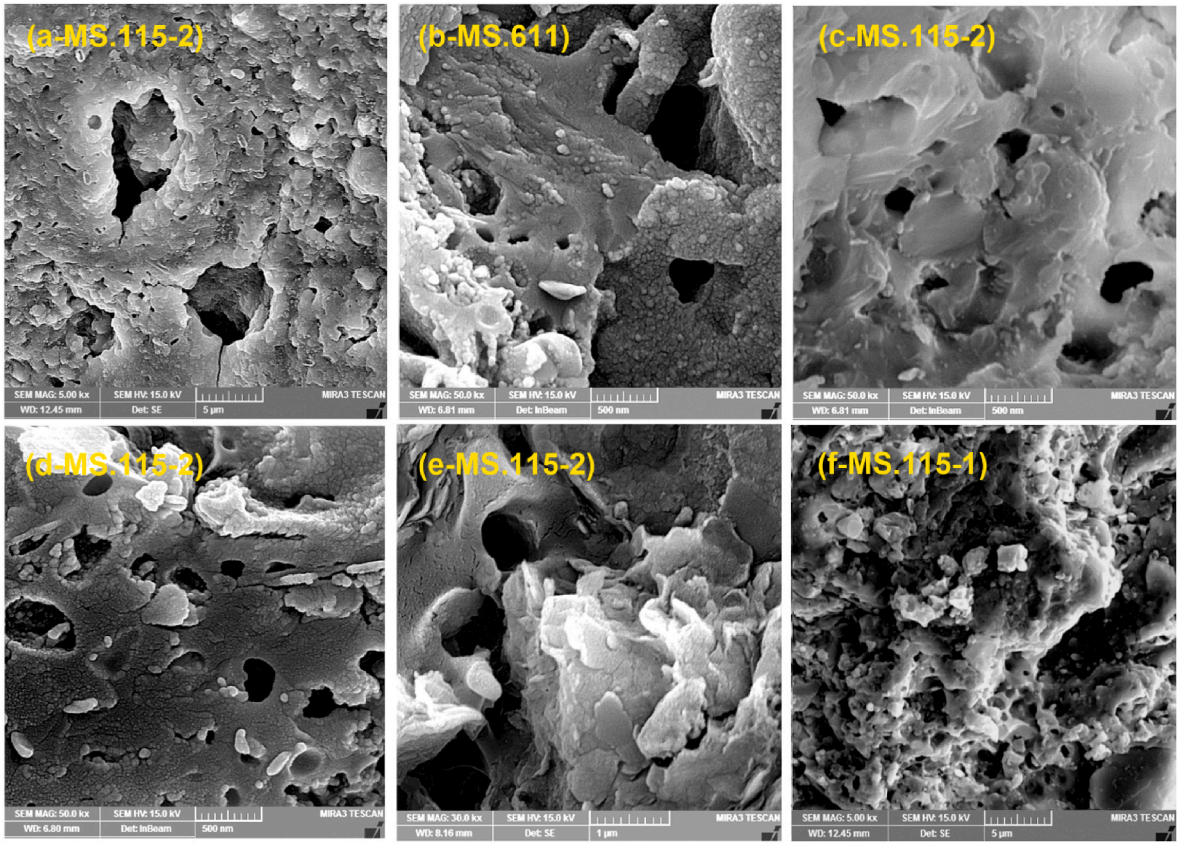


Fig. 6. FE-SEM images of rounded pores in sample MS.611, suggesting at initial sintering process of the clay body at ~800 °C and the increases of bubbles >0.005 μm in the samples MS.115–1 and MS.115-2 due to the partial melting of phyllosilicates and the formation of glassy phase from 950 °C.

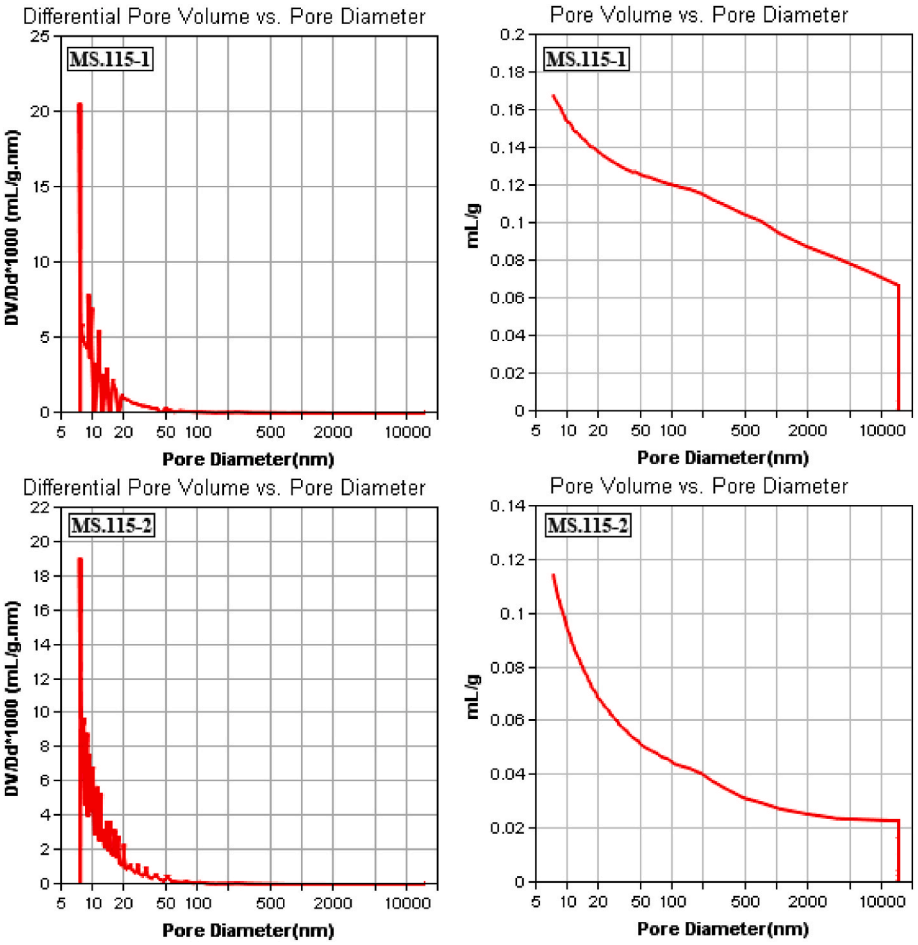


Fig. 7. Cumulative pore volume and pore size distribution of fine-grained wares, showing the volume of intruded mercury (mL/g) in a maximum applied pressure P (kg/cm2) of sample MS.115–1 and MS.115–2.

with subsequent pores formation, and the firing temperature reached is not sufficient to develop synthetization of the matrix. Additionally, the use of coarse temper greatly contributed to the high extent of meso-and macro-pores and the non-uniform distribution of larger pores in the sample. The pore size distribution of sample MS.120 displays, indeed, the abundance of pores larger than 10 μm (Fig. 8). The broad pore distribution refers to an unvitrified structure confirmed by FE-SEM observations. The addition of organic materials, indeed, highly increases the mesoporosity during combustion since its effect is twofold forming new pores and enhancing the sintering process [15]. Also, the presence of fractures in the coarse mineral grains implies the initiation of a fusion process, increasing the total pore volume [6]. In the coarse ware of MS.120, the mixed material exhibits a poly-modal pore distribution in an interval from 200 nm to 15 μm attributed to the addition of coarse particles (Dutra, 2019). While sample MS.611 shows a bimodal distribution at around 8 μm and 50 μm, due to the more developed microstructures caused by the dissolution of the carbonate that is taking place [41]. Also, total porosity values in samples MS.120 and MS.611 are very different. Sample MS.120 displays 19.96% of porosity while sample MS.611 has a total percentage of 5.67% (Table 1). The lower porosity of sample MS.611 confirms the similarity with sample MS.115–2, characterized by a high degree of vitrification of the matrix.

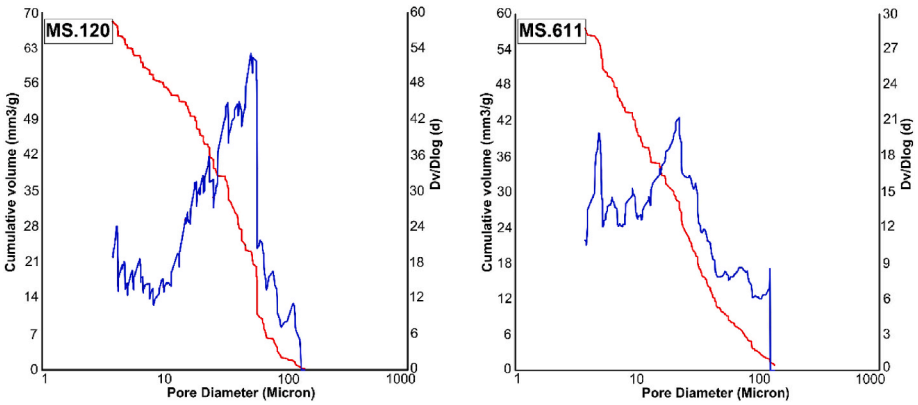


Fig. 8. Cumulative pore volume and pore size distribution of the samples MS.120 and MS.611.

The results indicated a distinctive contrast in the pore structures and total porosity of the samples which can be related to the use of different firing processes and diverse types of chemical and mineralogical compositions from the fifth to fourth millennium BC.

3.3. Cold crushing strength (CCS)

The CCS results show different important factors such as total porosity and firing temperature, influencing the crushing strength of the ceramics (Table 1). CCS values represent the mean value which was obtained from the same sherd. The CCS shows a range of crushing strength from 6.31 MPa to 16.5 MPa at different porosities from 5% to 1 9% respectively (Table 1). The low-fired ceramic samples MS.120 and MS.611 with different typological variants had the lowest cold crushing strength of 6.24 MPa and 6.31 MPa at a temperature <700 °C and ~750 °C. The sample MS.120 with the lowest crushing strength had maximum porosity of 19.96%, while porosity started decreasing from ≥750 °C. The low-fired ceramic (samples MS.120 and MS.611) had lower fracture energy of 2635 and 4413 (Table 1). However, The crushing strength value in texturally more homogeneous samples such as samples MS.115–1 and MS.115–2 at 850–900 °C sintering temperature was higher than the low compactness samples. The fracture energies were 10,424 and 6926 for samples MS.115–2 and MS.115–1, respectively (Table 1). This indicates that both porosity and sintering temperatures play a significant role in determining their crushing strength. The beginning of gehlenite crystalization in sample MS.115–2 was also responsible for its high strength (Amkpa et al., 2017). The Al_2O_3 (Alumina) reacted with CaO during the firing process increasing the strength of the clay material (Amkpa et al., 2017).

4. Discussions

In this study, a specific representative subset of ceramics found in burial and settled conditions of the site effectively evaluated the suitability of the integrated porosimeter for accessing the desired pore size distribution range without considering the pore fraction. The combined approach adopted for studying porosity was useful in order to investigate pores and microstructure at different scales. MIP and FESEM results, indeed, show the increase of round cryptopores varying in the range of 10–500 nm at 950 °C, closely linked to the formation of glassy phases with bubbles. Whereas, a greater number of interconnected and corona-shaped pores was clearly evident in samples MS.611 and MS.115–2, partially sintered at ~750 and 850 °C, respectively. It indicates that the cryptopores (0.01–0.1 μm) thermally increased during the sintering process at around 950 °C. The results show that the different distribution of pore size and connectivity of pore system within the clay matrices can clearly discriminate the microstructure of ceramics. The subsequent removal of organic materials, loss of bonded water, decomposition of mineral phases, manufacturing process, the selection of angular compositions, and even the presence of intra-grain voids considerably influence the characteristics of pores and consequently decrease the surface resistance and mechanical strength of ceramic material [4,37]. The porosity of the samples was also greatly influenced by the mineralogical compositions and their transitions, contributing to the development of heat cracks, and interconnected and corona-shaped pores during the heating and cooling processes. The occurrence of carbonates in the raw material greatly contributed to the fissures and pores development under 1 μm between 800 and 1000 °C (Cultrone et al., 2004).

The porosity and physico-mechanical stability are the key properties for effective conservation of archaeological objects. Therefore, the strength of ceramics was distinctly obtained at two ranges of porosity and firing temperatures of 750–800 °C and 800–950 °C. Indeed, the crushing strength of the samples varies between 6 MPa and 16 MPa strictly depending on different groups of pore and crack initiators. The ceramics with less porosity and homogenous extended glassy phase exhibit higher strength values [8]. It shows that the crushing strength increases with decreasing in porosity. The ceramics with a great number of cryptopores in a range of 0.01–0.1 μm exhibit a higher value of crushing strength due to the decrease of primary porosity during the melting process (Duttra, 2016). The high-fired samples MS.115–1 and MS.115–2, vitrified up to a glassy network present low porosity in the range of 5–8% as well as the pore size in the range of nanometer-scale depending on the sintering temperature and the content of raw materials. On the other hand, an increase in sintering temperature leads to stronger bonding between particles and consequently to higher strength of final products [1,43]. Therefore, the extent of vitrification can mainly affect the measured strength values [1].

The ceramic produced from a carbonate-rich material and fired above 950 °C (sample MS.115–2) gives the highest strength value (16.5 MPa) due to the bond between two touching particles. Small particles bond together at a high sintering process and lead to a sustainable ceramic material with a uniform cross-section >900 °C. The occurrence of vitrified glassy connections between particles through the melting process and low interconnectivity increases the ceramic strength (Hein et al., 2018). Small pores connecting the large pores disappeared at the initial sintering stage which cause a dramatic increase in the crushing strength of the ceramics. Additionally, the formation of new silicate phases, such as gehlenite and diopside, in the sintered matrix and the development of effective porosity improve the crushing resistance of the high-fired ceramics. However, the strength of ceramics decreases depending on the particle size distribution and interconnections. The low crushing strength of coarse wares can be related to the increase in crack porosity area with high interconnectivity. The pore structures either in the form of closed corona-shaped pores around the mineral grains or interconnected channels can easily affect the strength of ceramics.

The low-fired ceramic with 19% (sample MS.120) porosity and a large number of interconnected pores meet a very low strength value (6.24 MPa). Higher porosity in these coarse-grained samples refers to the generation of crack porosity and a large number of through-fibrous pores, decreasing the surface resistance [4]. It shows that both pore and inclusion mainly affect the ceramic's strength [2]. The ceramic containing a high amount of primary calcite content exhibits lower strength [8]. The released CO_2 at 750 °C caused higher porosity and decreased the strength of the ceramic [44]. Additionally, in the coarse-tempered wares, an increased shrinkage of the clay matrix at higher temperatures results in weak bonding strength [1].

5. Conclusions

This study showed that the technological features such as hardness, total porosity, pore size distribution, and cumulative and relative pore volume of the ceramics can be a function of sintering temperature, fusion process, and type of temper selection. Therefore, the diversity in the pore structures and the range of porosity between the vessels can be clearly related to the technological variations from the fifth to fourth millennium BC in the central plateau of Iran.

The thermal analysis demonstrated the mineral transition temperatures and their effect on the crushing strength and porosity of the ceramics. Crystallization of the glassy phase increased the connectivity of the pore system and provided a less porous structure >950 °C which considerably increases the crushing strength and durability of the ceramics. However, the addition of coarse-grained particles increases the mean pore size. The porous ceramics containing high phyllosilicate grains were less resistant to crushing tests than the sintered compact wares. It shows that the pore network and the sintering process can mainly affect the strength of the materials. The results significantly contribute to the development of long-term stability of ceramic materials and prevent their biological and chemical weathering.

Declaration of competing interest

The authors declare that they have no known competing financial interests or personal relationships that could have appeared to influence the work reported in this paper.

Acknowledgments

The authors would like to kindly thank Behruz Karimi Shahraki from IMPRC and Javad Bakhtiyari from the Research Institute of Petroleum Industry for their help. We are deeply grateful to Roohollah Bagherzadeh from ATMT Research Institute, Textile Engineering Department, Amirkabir University of Technology, Tehran for his invaluable advice for mercury intrusion analysis. This research did not receive any specific grant from any funding agencies. The ceramics had been supplied by the project of archaeological excavation of Mulavi Street in Tehran, funded by the Iranian Cultural Heritage Organization in Tehran.

References

[1] M.S. Müller, V. Kilikoglou, P.M. Day, G. Vekinis, The influence of temper shape on the mechanical properties of archaeological ceramics, J. Eur. Ceram. Soc. 30 (2010) 2457–2465.
[2] K. Alexiou, N.S. Müller, I. Karatasios, V. Kilikoglou, The performance of different adhesives for archaeological ceramics under mechanical stress, Appl. Clay Sci. 82 (2013) 10–15.
[3] C. Coletti, G. Cultrone, L. Maritan, C. Mazzoli, Combined multi-analytical approach for study of pore system in bricks: how much porosity is there? Mater. Char. 121 (2016) 82–92.
[4] G. Pia, C. Siligardi, L. Casnedi, U. Sanna, Pore size distribution and porosity influence on Sorptivity of ceramic tiles: from experimental data to fractal modelling, Ceram. Int. 42 (2016) 9583–9590.
[5] M. Hasanuzzaman, R A R M, A.G. Harunur, Olabi, Characterization of porous glass and ceramics by mercury intrusion porosimetry, Ref. Mod. Mater. Sci. Mater. Eng. (2017) 1–9.
[6] L.F. Dutra, M.E. Freitas, A. Grillet, N. Mendes, M. Woloszyn, Microstructural characterization of porous clay-based ceramic composites, Materials 12 (946) (2019) 1–16.
[7] W.A. Kahl, B. Ramminger, Non-destructive fabric analysis of prehistoric pottery using high-resolution X-ray microtomography: a pilot study on the late Mesolithic to Neolithic site Hamburg-Boberg, J. Archaeol. Sci. 39 (2012) 2206–2219.
[8] E. Tsantini, E. Jiménez-Piqué, G. Montana, L. Randazzo, Strength of pre-Roman amphorae: comparison of the different types, J. Archaeol. Sci.: Report 2 (2015) 405–417.
[9] F. Turco, P. Davit, R. Cossio, A. Agostino, L. Operti, Accuracy improvement by means of porosity assessment and standards optimization in SEM-EDS and XRF elemental analyses on archaeological and historical pottery and porcelain, J. Archaeol. Sci.: Report 12 (2017) 54–65.
[10] G. Giacosa, D. Moro, G. Ulian, S. Zanna, G. Valdrè, Ceramic recipes: cross-correlated analytical strategy for the characterization of the iron age pottery from ancient karkemish (Turkey), Measurement 128 (2018) 180–188.
[11] M. Hasanuzzaman, A. Rafferty, A.G. Olabi, Effects of zircon on porous structure and alkali durability of borosilicate glasses, Ceram. Int. l40 (2014) 581–590.
[12] P.E. Dim, R.S. Fletcher, S.P. Rigby, Improving the accuracy of catalyst pore size distributions from mercury porosimetry using mercury thermoporometry, Chem. Eng. Sci. 140 (2016) 291–298.
[13] M. Von Bradke, F. Gitzhofer, R. Henne, Porosity determination of ceramic materials by digital image analysis–A critical evaluation, Scanning 27 (2005) 132–135.
[14] C. Coletti, G. Cultrone, L. Maritan, C. Mazzoli, How to face the new industrial challenge of compatible, sustainable brick production: study of various types of commercially available bricks, Appl. Clay Sci. 124–125 (2016) 219–226.
[15] C. Coletti, E. Bragié, M.C. Dalconi, C. Mazzoli, A. Hein, L. Maritan, A new brick-type using grape stalks waste from wine production as pore-agent, Open Ceramics (2023), 100365, https://doi.org/10.1016/j.oceram.2023.100365.
[16] M.E. Esmaeili Jelodar, The first possible evidence of the A ceramic neolithic in the Iranian central plateau, Antiquity 92 (4) (2018) 1–8, 362.
[17] S. Lu, X. Yu, Y. Zong, Nano-microscale porosity and pore size distribution in aggregates of paddy soil as affected by long-term mineral and organic fertilization under ricewheat cropping system, Soil Tillage Res. 186 (2019) 191–199.
[18] K. Elaiopoulos, T. Perraki, E. Grigoropoulou, Mineralogical study and porosimetry measurements of zeolites from Scaloma area, Thrace, Greece, Microporous Mesoporous Mater. 112 (2008) 441–449.
[19] E.W. Washburn, The dynamics of capillary flow, Phys. Rev. 17 (1921) 273–283.
[20] G. Njiekak, D.R. Schmitt, R.S. Kofman, Pore systems in carbonate formations, Weyburn field, Saskatchewan, Canada: micro-tomography, helium porosimetry and mercury intrusion porosimetry characterization, J. Petrol. Sci. Eng. 171 (2018) 1496–1513.
[21] W. Hai-tao, K. Ling-xue, B. Jin, B. Zong-qing, L. Dong-mei, L. Wen, Transformation of minerals in direct coal liquefaction residue under gasification atmosphere at high temperatures, J. Fuel Chem. Technol. 43 (3) (2015) 257–265.
[22] E. Rayóna, M.P. Arrieta, T. Pasíes, J. López, J.L. Jordá, Enhancing the mechanical features of clay surfaces by the absorption of nano-SiO_2 particles in aqueous media. Case of study on Bronze Age clay objects, Cement Concr. Compos. 93 (2018) 107–117.
[23] M. Daghmehchi, C. Rathossi, H. Omrani, M. Emami, M. Rahbar, Mineralogical and thermal analyses of the hellenistic ceramics from laodicea temple, Iran, Appl. Clay Sci. 162 (2018) 146–154.
[24] D.H. Moon, S.J. Kim, S.W. Nam, H.G. Cho, X-Ray diffraction analysis of clay particles in ancient baekje black pottery: indicator of the firing parameters, Minerals 11 (1239) (2021) 1–11.
[25] L. Nodari, E. Marcuz, L. Maritan, C. Mazzoli, U. Russo, Hematite nucleation and growth in the firing of carbonate-rich clay for pottery production, J. Eur. Ceram. Soc. 27 (2007) 4665–4673.
[26] P. Ricciardi, P. Colomban, V. Milande, Non-destructive Raman characterization of capodimonte and buen retiro porcelain, J. Raman Spectrosc. 39 (2008) 1113–1119.
[27] R. Annamalai, G. Ravisankar, R. Naseerutheen, A. Chandrasekaran, K. Rajan, Application of various spectroscopic techniques to characterize the archaeological pottery excavated from Manaveli, Puducherry, India, Optik 125 (2014) 6375–6378.
[28] A. Grunenwald, C. Keyser, A.M. Sautereau, B. Ludes, E. Crubezy, C. Drouet, Revisiting carbonate quantification in apatite (bio)minerals: a validated FTIR methodology, J. Archaeol. Sci. 49 (2014) 134–141.
[29] M. Daghmehchi, A. Guido, A. Mastandrea, M.A. Salahi, M. Omrani, J. Nokandeh, Thermal analysis of ancient ceramics using the microchemical and microstructural alterations of foraminifera, Mater. Char. 130 (2017) 81–91.
[30] G.T. Zhou, Y.B. Guan, Q.Z. Yao, S.Q. Fu, Biomimetic mineralization of prismatic calcite mesocrystals: relevance to biomineralization, Chem. Geol. 279 (2010) 63–72.
[31] L. Medeghini, S. Mignardi, C.D. Vito, A.M. Conte, Evaluation of a FTIR data pretreatment method for principal component analysis applied to archaeological ceramics, Microchem. J. 125 (2016) 224–229.
[32] L. Damjanovic, I. Holclajtner-Antunovic, U.B. Mioc, V. Bikic, D. Milovanovic, I. Radosavljevic Evans, Archaeometric study of medieval pottery excavated at Stari (Old) Ras, Serbia, J. Archaeol. Sci. 38 (2011) 818–828.
[33] M. Daghmehchi, B. Karimi Shahraki, H. Omrani, M. Madanipour, M.A. Emami, J. Nokandeh, H. Omrani Rekavandi, E.W. Sauer, Ancient Arms Race: antiquity's largest fortresses and Sasanian military networks of northern Iran, in: Chemical and Vibrational Spectroscopic Analyses of Similar Types of Vessels from Forts on the Great Wall of Gorgan and Fortifications in its Hinterland, Oxbow publisher, 2022.
[34] L. Maritan, L. Nodari, C. Mazzoli, A. Milano, U. Russo, Influence of firing conditions on ceramic products: experimental study on clay rich in organic matter, Appl. Clay Sci. 31 (2006) 1–15.
[35] M. Emami, R. Trettin, Mineralogical and chemical investigations on the ceramic technology in Čoğā Zanbil,(Iran, 1250 BC), Period. Mineral. 81 (3) (2012) 359–377.
[36] G. Velraj, K. Janaki, A. Mohamed Musthafa, R. Palanivel, Spectroscopic and porosimetry studies to estimate the firing temperature of some archaeological pottery shreds from India, Appl. Clay Sci. 43 (2009) 303–307.
[37] C. Volzone, N. Zagorodny, Mercury intrusion porosimetry (MIP) study of archaeological pottery from Hualfin Valley, Catamarca, Argentina, Appl. Clay Sci. 91–92 (2014) 12–15.
[38] M. Emami, R. Chapoulie, K. Abdi, Cathodoluminescence microscopy for interpreting the fabric and heating process of ancient pottery: preliminary study on the technological features of pottery from the Kur River basin, Archaeometry (2021) 1–20.
[39] M. Daghmehchi, H. Omrani, M. Emami, J. Nokandeh, Mineralogical and thermo-chemical characteristics of the Hellenistic ceramics and raw clay from Qizlar Qal'eh (northeastern Iran), Mater. Char. 120 (2016) 143–151.
[40] C. Coletti, L. Maritan, G. Cultrone, M.C. Dalconi, A. Hein, E. Molina, C. Mazzoli, Recycling trachyte waste from the quarry to the brick industry: effects on physical and mechanical properties, and durability of new bricks, Construct. Build. Mater. 166 (2018) 792–807.
[41] E.M. Pérez-Monserrat, L. Maritan, E. Garbin, G. Cultrone, Production technologies of ancient bricks from Padua, Italy: changing colors and resistance over time, Minerals 11 (744) (2021) 1–29.
[42] K. Guan, W. Qin, Y. Liu, X. Yin, C.L.M. Peng, Q. Sun, J. Wu, Evolution of porosity, pore size and permeate flux of ceramic membranes during sintering process, J. Membr. Sci. 520 (2016) 166–175.
[43] M.F. Zawrah, R.M. Khattab, L.G. Girgis, E.E. ElShereefy, S.E. AboSawan, Effect of CTAB as a foaming agent on the properties of alumina ceramic membranes, Ceram. Int. 40 (2014) 5299–5305.
[44] B. Abdelmalek, B. Rekia, B. Youcef, B. Lakhdar, F. Nathalie, Mineralogical characterization of Neogene clay areas from the Jijel basin for ceramic purposes (NE Algeria-Africa), Appl. Clay Sci. 136 (2017) 176–183.